Backbone Dynamics of Human Cu,Zn Superoxide Dismutase and of Its Monomeric F50E/G51E/E133Q Mutant: The Influence of Dimerization on Mobility and Function†

Lucia Banci, Ivano Bertini,* Fiorenza Cramaro, Rebecca Del Conte, Antonio Rosato, and Maria Silvia Viezzoli

Department of Chemistry and Centro di Risonanze Magnetiche, University of Florence, Via Luigi Sacconi 6, 50019, Sesto Fiorentino, Italy

Received January 12, 2000; Revised Manuscript Received May 3, 2000

ABSTRACT: The backbone assignment of reduced human dimeric Cu,Zn superoxide dismutase (SOD) was performed on a sample 100% enriched in ^{15}N, ^{13}C and 70% enriched in ^{2}H. ^{15}N T_1, T_2, and $T_{1\rho}$ and ^{15}N-^{1}H NOE assignment was performed at 600 MHz proton frequency on both wild-type SOD and the monomeric F50E/G51E/E133Q mutant. This allowed a comparison of the mobility in the subnanosecond and in the millisecond to microsecond time scales of the two systems. Both proteins are rather rigid, although some breathing of the β sheets is detected in the wild type dimer. The monomer displays large mobility in the loops in the first part of the sequence, in loop IVa where point mutations have been introduced and at the C-terminus. The dimeric wild type is rigidified at loop IVa and at the C-terminus. Only loop VII shows a higher mobility in the dimer (besides some individual NH moieties). Conformational equilibria are displayed in the monomeric form around cysteines 57 and 146, thus explaining the disorder of arginine 143 which is the most important residue in guiding O_2^- toward the copper ion. The larger mobility in the wild type form with respect to the monomer in the picosecond to nanosecond time scale of helix α1 and loop VIIb, which provides the correct electrostatic driving force for O_2^- in the active channel, has been discussed in terms of favoring the activity of SOD.

The dynamic properties of biological macromolecules are as important with respect to their function as their average structural properties. The present investigation aims at characterizing the dynamic properties in both the dimeric and monomeric forms of human SOD[1] through the analysis of heteronuclear relaxation rates.

Copper/zinc superoxide dismutase (SOD) is a metalloprotein that is found in almost all eukaryotic cells and in a few prokaryotes (*1*). This protein catalyzes the dismutation of the superoxide radical to hydrogen peroxide and oxygen according to the following reactions (*2*, *3*):

$$Cu^{2+} + O_2^- \rightarrow Cu^{1+} + O_2$$

$$Cu^{1+} + O_2^- \rightarrow Cu^{2+}(O_2^{2-}) \xrightarrow{2H^+} Cu^{2+} + H_2O_2$$

The copper ion is the catalytic center. The zinc ion may play both a structural role and a role in determining the electrostatic field of the protein, by providing a further positively charged center close to the active site. The copper ion lies at the bottom of a wide channel that is 10 Å deep (*4*). The side chains of the residues in the active site channel determine a positive electrostatic field**,** which plays a critical role in attracting anions, guiding them into the channel to the copper ion and determining the catalytic rates (*5*−*9*).

All the intracellular eukaryotic SODs are dimeric, with two identical subunits held together by hydrophobic interactions (*10*, *11*), and have a very well conserved folding topology. Each subunit of human SOD has 153 amino acids arranged in a β barrel structure composed of eight antiparallel β strands. The strands are connected by loops of various lengths, which have been numbered according to the number of the first strand they connect. The loops with an even number are involved in interactions between the two subunits, while among the loops with an odd number, the important loop VII (the so-called electrostatic loop) is present. The latter loop contains several charged residues which produce an electrostatic field suitable to guide the superoxide anion to the copper ion (*7*).

Monomeric forms of the enzyme have been obtained by substituting hydrophobic residues at the subunit−subunit interface with hydrophilic residues. In particular, Phe 50 and Gly 51 have been substituted by two Glu residues, yielding a soluble single subunit (*12*). The enzymatic activity of this mutant, however, is quite reduced with respect to the native form, i.e., to 10% (*12*). Therefore, to partially restore the activity, Glu 133 has been neutralized by substituting it with Gln (*13*). This mutation on the native protein doubles the activity (*6*); the same occurs also on the present monomeric form (*13*). From now on, the expression "monomeric SOD" will refer to the partially active F50E/G51E/E133Q monomeric triple mutant. The solution (*14*) and solid state (*15*) structures of this monomeric protein have been recently

† This work was supported by the European Union (Large Scale Facility Grant ERBFMGECT950033), by MURST ex 40%, and by CNR_Progetto Finalizzato Biotechnologie (99.00286.PF49).

* To whom correspondence should be addressed. Phone: +39 055 4209272. Fax: +39 055 4209271. E-mail: bertini@cerm.unifi.it.

[1] Abbreviations: SOD, superoxide dismutase; WT, wild-type; NMR, nuclear magnetic resonance; TPPI, time proportional phase increments.

10.1021/bi000067z CCC: $19.00
Published on Web 07/14/2000

reported. The global fold of monomeric SOD was shown to be essentially the same as that of a single subunit of the WT enzyme. Specific structural differences in the active channel have been found and proposed to be responsible for the diminished catalytic activity of monomeric SOD with respect to the WT enzyme (*14*).

The observed rates for the catalyzed reaction are very fast, $\sim(2-3) \times 10^9$ M^{-1} s^{-1} (*16*−*18*), and in non saturating concentrations of the substrate are limited by the diffusion of the superoxide anion in the active channel to the copper ion. Several studies on proteins mutated on residues in the active site channel as well as activity measurement as a function of ionic strength have supported the proposed major role of electrostatic forces in driving and in enhancing the affinity of the substrate to the reaction cavity (*5*, *6*, *19*−*22*). Simulation through Brownian dynamics calculations (*23*), which allowed calculation of the rate of the enzyme/substrate reaction and factorization of the various contributions, were consistent with experimental studies indicating that the diffusion of superoxide is enhanced by the positive electrostatic potential produced by the residues at the active site channel. Fluctuations of the active site residues can therefore reflect in fluctuation of this positive electrostatic potential field, thus affecting the overall enzymatic reactivity.

Through ^{15}N relaxation measurements, a detailed description of protein backbone motions, at the level of individual residues can be obtained (*24*−*27*). Results are usually interpreted in terms of the so-called model-free approach (*28*) or as values of the spectral density function at various frequencies (*29*). In the present study, available expressions for the spectral density functions derived for the case of anisotropic protein tumbling (*30*) were used in conjunction with the model-free approach to derive motional parameters (*31*, *32*). A proper treatment of the anisotropy of molecular reorientation in solution is of course very important when comparing the dynamic properties of a monomeric and a dimeric system, as such anisotropy is somewhat different in the two systems. Motional parameters derived without taking this into account could not be compared meaningfully (*31*). On the other hand, the information on molecular motions occurring on the microsecond to millisecond time scale obtained from off-resonance $R_{1\rho}$ measurements is not affected by the anisotropy of molecular reorientation.

In the present research, the measurement of R_1, R_2, hetero-NOE, and off-resonance $R_{1\rho}$ relaxation data for all backbone amide nitrogens on the reduced state for both forms are reported and analyzed. The first three sets of data provide information on backbone mobility in the picosecond to nanosecond time scale (*24*, *25*, *28*, *29*), whereas the latter set of data provides information on backbone mobility in the microsecond to millisecond time scale (*27*, *33*). The comparison of the dynamic properties of the dimeric and monomeric forms of human SOD complements the static structural comparisons already available (*14*, *15*), and provides further and complementary information on the reasons for the lower activity of the monomer and on the mechanisms of enzymatic activity.

EXPERIMENTAL SECTION

Sample Preparation. The monomeric mutant and dimeric human SOD have been expressed in *Escherichia coli* TOPP1 strain (Stratagene) as previously reported to obtain ^{15}N labeled monomeric and dimeric proteins (*13*). For the dimeric protein also a ^{15}N, ^{13}C, ^{2}H labeled sample was obtained by growing the cells in minimal medium (M9) containing 0.6 g/L ^{15}N ammonium sulfate, 2 g/L ^{13}C glucose, 80% $^{2}H_2O$. The samples were isolated and purified according to previously published protocols (*6*). The single labeled samples were fully enriched in ^{15}N while the triple labeled dimeric SOD was fully enriched in ^{15}N and ^{13}C and contained about 70% ^{2}H. Reduction was achieved by addition of sodium isoascorbate to a final concentration of about 4−6 mM, in 20 mM phosphate buffer at pH 5.0 under anaerobic conditions. The NMR samples had a concentration of about 2 mM and contained 10% D_2O for the lock signal.

NMR Experiments. The NMR experiments for the backbone assignment of the dimeric human SOD were recorded on a Bruker Avance 800 spectrometer operating at 18.7 T. All experiments were performed with a triple-resonance 5 mm probe, with a BGU unit for the self-shielded z-gradient and with a lock switch unit, at 298 K on the ^{15}N, ^{13}C, ^{2}H-labeled sample. Constant time HNCA (*34*), NH(CO)CA (*34*), HNCO (*34*), and HN(CA)CO (*35*)-TROSY (*36*) three-dimensional, triple resonance experiments and two-dimensional ^{15}N-HSQC spectra were collected. The spectral windows used in the HNCA and HN(CO)CA were 11363 Hz (^{1}H) × 3333 Hz (^{15}N) × 6250 Hz (^{13}C) using, respectively, 1024 (^{1}H) × 40 (^{15}N) × 256 (^{13}C) and 1024 (^{1}H) × 40 (^{15}N) × 320 (^{13}C) data points. The HNCO and HN(CA)-CO-TROSY-type experiments were collected with spectral windows of 11240 Hz (^{1}H) × 3280 Hz (^{15}N) × 2499 Hz (^{13}C) using, respectively, 1024 (^{1}H) × 40 (^{15}N) × 192 (^{13}C) and 1024 (^{1}H) × 40 (^{15}N) × 320 (^{13}C) data points.

A ^{15}N-NOESY-HSQC (*37*) was also performed at 298K, on a ^{15}N labeled sample of dimeric SOD. The spectrum was recorded at 800 MHz with spectral windows of 9569 Hz (^{1}H) × 2989 Hz (^{15}N) × 10403 Hz (^{1}H) for 2048 (^{1}H) × 88 (^{15}N) × 296 (^{1}H) data points.

For all spectra shifted sine bell functions were used to apodize the data. The data were zero-filled once in indirect dimensions before Fourier transformation.

All NMR experiments for determination of ^{15}N longitudinal and transversal relaxation rates and ^{1}H-^{15}N NOE were recorded at 298 K on a 600 Bruker Avance spectrometer (for both the monomeric and the dimeric species). Experiments were performed with a 5 mm inverse probe (for the monomer) and a 5 mm triple-resonance probe (for the dimer) on samples enriched only in ^{15}N.

^{15}N R_1 relaxation rates were measured using an already reported sequence (*29*), modified to remove cross correlation effects during the relaxation delay (*38*). 2048 × 200 data points were collected using 8 scans for each experiment. The recycle delay was 1.8 s for monomeric SOD, and 3.0 s for the WT dimeric enzyme plus an acquisition time of 142.6 ms for both of them. Spectral windows were 7183 Hz (^{1}H) × 2016 Hz (^{15}N) for the monomeric SOD and 7184 Hz (^{1}H) × 2688 Hz (^{15}N) for the dimeric protein. Data were zero-filled to obtain 2048 × 512 data point matrixes. A commercially available algorithm for linear prediction was used in the indirect dimension to increase resolution. Quadrature detection in the F1 dimension was obtained using the TPPI (*39*) method. Presaturation was used to suppress the strong solvent signal. For monomeric SOD, 10 experiments were

collected to measure the ^{15}N R_1 relaxation rates, with recovery delays of 10, 70, 150, 250, 380, 540, 740, 1000, 1350, and 3000 ms. For WT dimeric SOD, thirteen experiments were collected, with recovery delays of 10, 70, 150, 250, 380, 450, 540, 740, 1000, 1350, 1650, 2000, and 3000 ms. ^{15}N R_2 relaxation rates at 14.1 T were measured by a commonly used pulse sequence (*24*, *38*). The experimental conditions used were the same as for the measurement of R_1, the only difference being that data points were collected using 16 scans. For monomeric SOD, nine experiments were carried out, using delays of 7.6, 15.2, 30.4, 53.2, 83.6, 121.6, 167.2, 228.0, and 304.0 ms. For WT dimeric SOD, ten experiments were collected, with recovery delays of 3.9, 7.7, 11.6, 15.4, 27.0, 42.4, 46.0, 53.9, 61.6, and 77.0 ms. ^{1}H-^{15}N NOEs were measured using a previously reported sequence (*40*). Data points were collected using 48 scans for both forms. ^{1}H saturation was maintained for 2.5 s. Water suppression was obtained using the water flip-back experimental scheme, which avoids water saturation (*40*). For both the monomer and the dimer, four spectra were performed: two spectrum with ^{1}H saturation and two without. Data were zero-filled to obtain 2048 × 512 data point matrixes. For the indirect dimension a commercially available algorithm for linear prediction was used and quadrature detection was applied using the TPPI (*39*) method.

Off-resonance rotating frame relaxation rates, $R_{1\rho}^{OFF}$ were measured as a function of the effective spin-lock power at 14.1 T using a previously reported pulse sequence (*41*). For monomeric SOD, $R_{1\rho}^{OFF}$ thirteen measurements were recorded at different effective spin-lock power values (the corresponding tilt-angles are given in parentheses): 4515 (25°), 4036 (35°), 3662 (35°), 3327 (35°), 3026 (35°), 2851 (33°), 2708 (35°), 2490 (50°), 2448 (35°), 2266 (50°), 2027 (50°), 1833 (50°), and 1632 Hz (50°), whereas for WT dimeric SOD seven experiments were performed at the following effective spin lock power values: 2179 (35°), 1801 (35°), 1638 (35°), 1503 (35°), 1361 (35°), 1125 (50°), and 919 Hz (50°). The effective spin lock power was varied either by varying the offset between the frequency at which the spin-lock was applied and the frequency corresponding to the center of the ^{15}N window (held constant) or by changing the applied B_1 field strength. In each measurement the duration of the trapezoid-shaped spin lock pulse was varied (10, 20, 36, 60, 86, 100, 150, 200, and 300 ms, respectively, in the dimeric SOD the first seven values were used). The conditions of acquisition used were the same of those used for R_2 measurements.

All NMR data were processed with the standard Bruker software packages (XWINNMR).

Resonance Assignment. The backbone assignment of monomeric SOD was taken from (*14*, *42*).

Assignment of the $^{1}H_N$, ^{13}C, ^{15}N NMR resonances of the backbone nuclei of dimeric SOD was carried out taking into account that the two subunits of the homo-dimer SOD show degenerate resonances. Therefore, signals for only 153 residues are expected. Most of the ^{1}H-^{15}N degeneracies present in ^{15}N-HSQC spectrum could be resolved in at least one of the HNCA, HN(CO)CA, HNCO of HN(CA)CO-TROSY-type spectra. The sequential assignment was performed combining, as also done for monomeric SOD (*42*), the assignment of the intraresidue $^{1}H_N(i)-^{15}N(i)-^{13}C\alpha(i)$, $^{13}CO(i)$ correlations with the sequential interresidue $^{1}H_N(i)-^{15}N(i)-^{13}C\alpha(i\text{-}1)$, $^{13}CO(i-1)$ correlations. The assignment were confirmed by the analysis of the sequential connectivities in the ^{15}N-NOESY-HSQC experiment.

Analysis of ^{15}N Relaxation Data. R_1, R_2, and $R_{1\rho}^{OFF}$ relaxation rates were determined by fitting the cross-peak volumes (I), measured as a function of the relaxation delay, to a single-exponential decay by using the Levenberg−Marquardt algorithm (*43*) as described in the literature (*44*). Uncertainties had been evaluated using a Monte Carlo approach (*44*). Heteronuclear NOE values were calculated as the ratio of peak volumes in spectra recorded with and without ^{1}H saturation. The heteronuclear NOE values and their errors were estimated by calculating the mean and the standard error from the available NMR data sets.

^{15}N relaxation data were analyzed in terms of the model-free formalism (*28*) through the Modelfree program, version 4.0, following the reported protocol (*45*), and by taking into account anisotropic reorientation as described in the Modelfree 4.0 manual and in ref *46*. An initial estimate of the diffusion tensor (**D**) of the molecule was obtained by fitting the local correlation times for the HN vector of each residue to an input structure (*46*, *47*) with the program *quadric_diffusion*, available from the world wide web site of Dr. A. G. Palmer III. The quality of the fit was measured by the χ^2 statistic:

$$\chi_{N-m}{}^2 = \sum_{i=1}^{N} \frac{(t_i - t_i^f)^2}{\sigma_i^2} \qquad (1)$$

where N is the number of the experimental data, m is the number of fitted parameters (equal to 1 for the isotropic diffusion model, 3 for the axially symmetric model, and 6 for the fully anisotropic model), t_i is the ith local correlation time, t_i^f is the corresponding fitted value, and σ_i is the uncertainty in t_i. The improvement in the fit afforded by the use of a second diffusion model with $n > m$ parameters is tested by using an F-statistic:

$$F_{n-m,N-n} = \frac{(\chi_{N-m}{}^2 - \chi_{N-n}{}^2)(N-n)}{\chi_{N-n}{}^2(n-m)} \qquad (2)$$

The statistical significance of the above test is determined by the probability p that the observed F value would be equaled or exceeded by random chance. If $p \leq \alpha$, then the obtained improvement is significant at the $(1-\alpha)$% confidence level.

Care was taken to remove from the input ^{15}N R_2 and R_1 data used for the evaluation of the diffusion tensor all amino acids having an exchange contribution to the R_2 value or exhibiting large-amplitude internal motions on a time scale longer than a few hundred picoseconds (identified from their low NOE value), as inclusion of these data would bias the calculated tensor parameters (*48*). The structures of monomeric and dimeric SOD used as input structures for *quadric_diffusion* and Modelfree calculations were the energy minimized average solution structure (PDB entry 1BA9) (*14*) and the crystal structure of the G37R mutant of the human enzyme (PDB entry 1AZV) (*49*), respectively. The latter structure is the one with the highest resolution available. To

check the stability of the results with respect to the input structure, calculations were run also using as input structures the X-ray structure of the reduced monomer (PDB entry 1MFM) (*15*) and of the wild-type human enzyme (PDB entry 1SPD) (*50*).

In the approach implemented in the Modelfree program, one can assume different models for internal motions, which correspond to assuming a different functional form (with a maximum of three adjustable parameters) for the spectral density functions $J(\omega)$ (which are used to recalculate the ^{15}N relaxation data). These are (under the assumption that the tumbling of the molecule in solution is isotropic)

$$J(\omega) = \frac{2}{5}\left[\frac{S^2\tau_m}{1+(\omega\tau_m)^2}\right] \quad (3a)$$

$$J(\omega) = \frac{2}{5}\left[\frac{S^2\tau_m}{1+(\omega\tau_m)^2} + \frac{(1-S^2)\tau'}{1+(\omega\tau')^2}\right] \quad (3b)$$

$$J(\omega) = \frac{2}{5}\left[\frac{S^2\tau_m}{1+(\omega\tau_m)^2} + \frac{(S_f^2-S^2)\tau'}{1+(\omega\tau')^2}\right] \quad (3c)$$

where $\tau'^{-1} = \tau_m^{-1} + \tau_e^{-1}$. The three adjustable parameters are S^2 (in eqs 3a−c), τ_e (in eqs 3b and 3c), and S_f^2 (in eq 3c). The model described by eq 3c, which is the most general, accounts for the presence of two distinct internal motions occurring on two different time scales. S^2 is the square of the generalized order parameter characterizing the amplitude of the internal motions, τ_m is the correlation time for molecular reorientation, τ_e is the correlation time for the slower internal motions, and S_f^2 is the square of the order parameter for the fast internal motions (having a correlation time much smaller than τ_e). Note that eqs 3b and 3a can be obtained from 3c assuming in the former case that $S_f^2 = 1$, and in the latter case that $S_f^2 = 1$ and τ_e is very small with respect to τ_m (in practice, smaller than a few tens of picoseconds). If an axially symmetric model is used to account for molecular rotational diffusion, the spectral density is given by (*30*, *51*, *52*)

$$J(\omega) = \frac{2}{5}\sum_{j=1}^{3} A_j\left[\frac{S^2\tau_j}{1+(\omega\tau_j)^2} + \frac{(S_f^2-S^2)\tau_j'}{1+(\omega\tau_j')^2}\right] \quad (4)$$

where $\tau_j'^{-1} = \tau_j^{-1} + \tau_e^{-1}$, $\tau_1^{-1} = 6D_\perp$, $\tau_2^{-1} = 5D_\perp + D_\parallel$, $\tau_3^{-1} = 2D_\perp + 4D_\parallel$, $A_1 = (3\cos^2\theta - 1)^2/4$, $A_2 = 3\sin^2\theta\cos^2\theta$, $A_3 = (3/4)\sin^4\theta$, and θ is the angle between the N−H bond vector and the principal axis of the diffusion tensor. All other symbols have the same meaning as above. Equation 4 corresponds to 3c. The expressions for $J(\omega)$ corresponding to eqs 3a and 3b can be derived from eq 4 as described above for the isotropic case.

To take into account the presence of a contribution to the experimental R_2 relaxation rate from conformational exchange processes, an additional adjustable parameter (R_{ex}), which sums up to the value of R_2 calculated taking into account only the dipolar and CSA contributions, may be introduced. As only three experimental data are available, the maximum number of adjustable parameters is three. Thus, R_{ex} can be introduced only in conjunction with models 3a and 3b (or their equivalent formulations including anisotropic rotational diffusion).

Fittings were performed by introducing upper limits for S^2 (≤ 1), S_f^2 (≤ 1) and τ_e ($< \tau_m$), and a lower limit for R_{ex} (> 0). No other restraints were used. Model selection in the Modelfree calculations was performed according to the procedure described in ref *45*, which is again based on χ^2 and F statistics (eqs 1 and 2). The uncertainties in the model-free parameter values were estimated by Monte Carlo simulations (*45*). In the last stage of calculations, for both the monomer and the dimer the τ_m value was optimized together with all other Modelfree parameters; for the dimer also the $D_\parallel/D_\perp$ ratio was optimized.

Off-resonance rotating frame relaxation rates are given by (*27*, *33*, *53*)

$$R_{1\rho}^{OFF} = R_1\cos^2\theta_i + R_{1\rho}^{ON,\infty}\sin^2\theta_i + K\sin^2\theta_i\frac{\tau_{ex}}{1+\tau_{ex}^2\omega_{eff,i}^2} \quad (5)$$

where R_1 is the longitudinal relaxation rate of the backbone ^{15}N nucleus of the ith residue, $R_{1\rho}^{ON,\infty}$ is the on-resonance rotating frame relaxation rate for an infinitely large effective field amplitude (where all exchange contributions are dispersed to zero), K is a constant equal to $p_a p_b \delta\Omega^2$, where p_a and p_b are the populations of the two states a and b between which the exchange process occurs, $\delta\Omega$ is the difference in the chemical shift of the ^{15}N in the two states, and τ_{ex} is the time constant for the exchange process. The effective field amplitude for the ith spin is $\omega_{eff,i} = (\Delta\omega_i^2 + \omega_1^2)^{1/2}$ where ω_1 is the amplitude of the applied RF irradiation, which is off-resonance with respect to the resonating frequency of the ith spin by an offset $\Delta\omega_i$. The angle $\theta_i = \arctan(\omega_1/\Delta\omega_i)$ is the angle between the effective magnetic field and the static magnetic field axes. It should be noted that eq 5 is valid in the limit of fast exchange with respect to the chemical shift separation, i.e., $\delta\Omega\cdot\tau_{ex} \ll 1$. As the angle θ_i is not equal for all spins, it is convenient to rearrange eq 5 as follows:

$$\frac{R_{1\rho}^{OFF} - R_1\cos^2\theta_i}{\sin^2\theta_i} = R_{1\rho}^{OFF,cor} = R_{1\rho}^{ON,\infty} + K\frac{\tau_{ex}}{1+\tau_{ex}^2\omega_{eff,i}^2} \quad (6)$$

The experimental $R_{1\rho}^{OFF,cor}$ values were fitted as a function of the amplitude of the effective applied spin-lock according to eq 6, where K and τ_{ex} were used as adjustable parameters. The $R_{1\rho}^{ON,\infty}$ value was fixed to the average value of $R_{1\rho}^{OFF,cor}$ for all residues not exhibiting a dependence on the applied spin-lock power (i.e., 13 s^{-1} for monomeric SOD and 30 s^{-1} for WT dimeric SOD). The range of spin lock powers applied sets the limits for the detection of conformational exchange processes, i.e., 15 $\mu s < \tau_{ex} < 200$ μs for the monomer and 35 $\mu s < \tau_{ex} < 350$ μs for the dimer.

RESULTS

Resonance Assignment of the Dimer. A total of 146 cross-peaks in the ^{15}N-HSQC spectra, which are identified as peptidic NH resonances, is observed out of the 147 expected signals, taking into account that the protein is a homodimer

Table 1: Rotational Diffusion Tensor Parameters for Monomeric and Dimeric SOD, Obtained Used Different Structures and/or Datasets for the *quadric_diffusion* Fittings (see text for details)

structure (PDB entry)	no. of data	D_{iso} ($/10^7$ s^{-1})	$D_{\|}/D_{\perp}$	reduced χ^2	*F*-test[a]	*P*[a]
monomer						
NMR (1BA9)	103	1.80 ± 0.01	1	3.82	1.87	0.14
X-ray (1MFM)	103	1.80 ± 0.01	1	3.82	1.36	0.26
dimer						
human X-ray (1SPD)	2×97	0.68 ± 0.01	1.18	11.9	6.54	0.0003
human G37R mutant (1AZV)	2×97	0.68 ± 0.01	1.29	10.3	17.6	$<10^{-6}$

[a] *F*-test values are reported for the comparison of the axial and the isotropic model for rotational diffusion. The value of the *F*-test is related to the probability (*p*) that the improvement in the fit observed when using the axial model occurs by chance.

where each subunit contains five prolines. A total of 139 of 147 expected sequential connectivities has been identified from the analysis of the HNCA and HN(CO)CA experiments and 132 have been determined from the analysis of the HNCO and HN(CA)CO-TROSY-type experiments.

The sequential assignment was performed using the interresidue connectivities available for $^{13}C\alpha$ and ^{13}CO nuclei. The assignment of these two nuclei for each residue together with the analysis of the sequential connectivities on the ^{15}N NOESY−HSQC maps allowed us to determine an unambiguous assignment for the backbone resonances of the 146 residues identified in the ^{15}N-HSQC spectra. Only the ^1H_N-^{15}N resonances of residue 64 could not be assigned.

The assignment for the backbone resonances (^1H_N, ^{15}N, $^{13}C\alpha$, and ^{13}CO) is reported in the Supporting Information.

Relaxation Measurements. ^{15}N relaxation data of monomeric and dimeric SOD are reported in the Supporting Information. In the case of monomeric SOD, it has been possible to obtain reliable values of R_1, R_2, and NOE values for 120 residues out of the 139 assigned backbone NH resonances. The signals of Leu 42, Thr 54, His 80, Ile 112, Val 119, and Val 148 were too weak to be integrated accurately, while those of Leu 8, Glu 21, Val 31, Glu 49, Phe 64, Lys 91, Asp 92, Asp 101, Leu 106, Thr 116, Gly 138, and Ile 149 were overlapped. Average values at 14.1 T of 1.41 ± 0.29 s^{-1} and 13.4 ± 6.3 s^{-1} for R_1 and R_2, respectively, were observed, while the average NOE value was of 0.81 ± 0.10. For dimeric SOD R_1, R_2, and NOE values were obtained for 117 residues out of 146 assigned backbone NH resonances. Residues Asp 52, Asn 65, Leu 67, Ile 112, and Thr 137 yielded signals too weak to allow accurate integration. The signals of the backbone NH of Lys 3, Ala 4, Val 5, Val 7, Gly 16, Glu 21, Glu 24, Ser 25, Trp 32, Leu 42, His 46, Val 47, Phe 50, Ser 59, Ser 68, Lys 70, Glu 77, Gly 85, Lys 91, Glu 100, His 120, Ser 134, and Gly 138 were overlapped. For dimeric SOD the average R_1, R_2 and NOE values, measured at 14.1 T, were 0.60 ± 0.11 s^{-1}, 33.9 ± 4.1 s^{-1}, and 0.81 ± 0.10 s^{-1}, respectively. These differences in the average values are consistent with what expected on the basis of the increase in the correlation time for the tumbling of the molecule (τ_m), occurring upon dimerization.

Rotational Diffusion Tensor. The inertia tensor (**I**) calculated for the average solution structure of the SOD monomer has principal values in the ratio 1.00:0.82:0.75, which compare well with those calculated from the X-ray structure of the monomer (1.00:0.83:0.76). From these values it is possible to estimate a $D_{\|}/D_{\perp}$ ratio of ca. 0.9. The above figures are calculated without taking into account the hydration shell of the protein, whose presence, as it is known, significantly reduces the anisotropy of rotational diffusion (*48*, *54*). It is thus expected that the rotational diffusion of the monomer be essentially isotropic. Indeed, as judged from χ^2 and *F*-test statistics (see Experimental Section), the individual local correlation times, estimated from the R_2/R_1 ratio of each residue, are satisfactorily fitted to the structure of the monomer using an isotropic model for rotational diffusion, and there is no statistically significant improvement of the fit by using a more complicated axial or fully anisotropic model (Table 1). The optimized value of D_{iso} is $(1.80 \pm 0.01) \times 10^7$ s^{-1}, corresponding to a correlation time for the molecular tumbling in solution ($\tau_m = 1/6D_{iso}$) of 9.3 ns. This value is consistent with what observed for other proteins of similar size (*45*).

For the dimer, the components of the inertia tensor are 1.00:0.95:0.43. The estimated $D_{\|}/D_{\perp}$ ratio is 1.8. Again, one should keep in mind that this is an upper limit for the actual $D_{\|}/D_{\perp}$ ratio, because hydration has not been taken into account. To estimate the parameters of the rotational diffusion tensor relative to the SOD dimer, residues in the model structure were numbered from 1 to 306. This structure was used to fit the correlation times of individual residues calculated from R_2/R_1 ratios, using duplicated data for residues 1−153 and 154−306. In this way, the data are fitted simultaneously to the two subunits, their reciprocal orientation being fixed to that observed in the input structure. The data are best fitted by an axial tensor with $D_{\|}/D_{\perp}$ ratio equal to 1.18 ± 0.02 if the structure of WT human SOD is taken as input structure or with a ratio of 1.29 ± 0.02 if the structure of the G37R mutant of human SOD (*49*) is used (Table 1). The lower χ^2 value obtained with the latter structure (Table 1) is an indication that it represents the structure in solution of the dimer better than the former. In all cases the optimized value of D_{iso} is $(0.68 \pm 0.01) \times 10^7$ s^{-1}, corresponding to a correlation time for the molecular tumbling in solution of 26 ns.

Figure 1 shows a view of the G37R mutant structure of the dimer from a direction orthogonal to the unique axis of the diffusion tensor. The reduced χ^2 is essentially the same for individual fittings to subunits A and B, and for the whole dimer, thus strongly indicating that the reciprocal orientation of the two subunits in the dimer in solution is the same as in the solid-state structure.

Modelfree and $R_{1\rho}$ Parameters. Figure 2 reports the parameters obtained from the Modelfree analysis of the ^{15}N relaxation data of the monomer. The data of 115 of 120 residues could be satisfactorily fit using the approach described in the Experimental Section. Relaxation data for residues 56, 67, 87, 113, and 126 were not fit well by any model; for final calculations, data for residues 67, 87, 113, and 126 were fit with the simplest model (described by eq

FIGURE 1: Display of the X-ray structure of G37R SOD seen from a direction orthogonal to the unique axis of the diffusion tensor ($\mathbf{D}_{||}$). The direction of the unique axis is shown by an arrow.

3a), and those for Gly 56 were fit with the same model, but using also R_{ex} as an adjustable parameter. This is justified by the fact that $R_{1\rho}$ measurements show that residue 56 is involved in a conformational equilibrium. The global value of τ_m was also optimized, yielding a final value of 9.10 ns. The overall average S^2 value is 0.89 ± 0.11. τ_e values were determined for residues 2, 10, 11, 12, 24, 26, 27, 34, 53, 55, 60, 68−70, 77, 84, 107, 141, 144, 151−153. S_f^2 values different from 1.00 were obtained for residues 11, 12, 24, 27, 34, 53, 55, 68, 107, 153. Residues 56, 61, 115, 118, 127, 146, and 147 exhibited a large (greater than 5 s^{-1}) R_{ex} contribution, arising from conformational exchange processes, to the transversal relaxation rate. Other 5 residues showed R_{ex} values lower than 5 s^{-1}. Conformational exchange was probed also by measuring the dependence of the ^{15}N relaxation rate in the rotating frame ($R_{1\rho}$) on the applied spin-lock power (*27*, *33*, *53*, *55*). Such a dependence was indeed observed for residues 56, 61, 115, 118, 146, and 147 in the Modelfree analysis. Residue 127 showed no dependence of $R_{1\rho}$ on the applied spin-lock power. However, its R_2 and average $R_{1\rho}$ values were larger than the average for the rest of the protein, indicating the presence of exchange processes on a time scale shorter than about 15 μs.

The results of the Modelfree analysis for the dimer are presented in Figure 3. ^{15}N relaxation data for 112 residues were fitted. Residues 6, 51, 55, 99, and 151 could not be fit satisfactorily by any model, and in final calculations were fitted with the simplest model (equivalent to eq 3a). For residue 151 also R_{ex} was used as an adjustable parameter. After the final optimization, the global value of τ_m was 25.3 ns and $D_{||}/D_{\perp}$ ratio was equal to 1.24 ± 0.02. The average S^2 value is 0.92 ± 0.09. τ_e values were determined for residues 2, 9, 10, 12, 14, 23, 26, 27, 37, 43, 49, 53, 56, 57, 75 (which cannot be seen in the figure, as the τ_e value is only about 10 ps), 78, 80, 102, 105−108, 128, 129, 133, 141, 142, 144, 145, 149, 150, 152, 153. S_f^2 values different from 1.00 are observed for residues 10, 12, 23, 26, 27, 37, 56, 108, 141, 153. R_{ex} values larger than 5 s^{-1} are obtained for residues 19, 20, 33, 45, 54, 89, 94, 104, 107, 126, 129, 145, 146. Other six residues had a R_{ex} value smaller than 5 s^{-1}. From the analysis of $R_{1\rho}$ rates, conformational exchange processes are detected for residues 19**,** 20, 54, 57, 58, 107, 117, 122, 126, 145, 151. For residue 33, no dependence of the measured $R_{1\rho}$ rates on the applied spin-lock power is detected; however, its R_2 value is significantly larger than the average R_2 for the rest of the protein, as well as than its average $R_{1\rho}$. This behavior is indicative of the presence of conformational exchange occurring on a time scale longer than 350 μs, but still fast with respect to the chemical shift difference of its amide ^{15}N between the conformers in

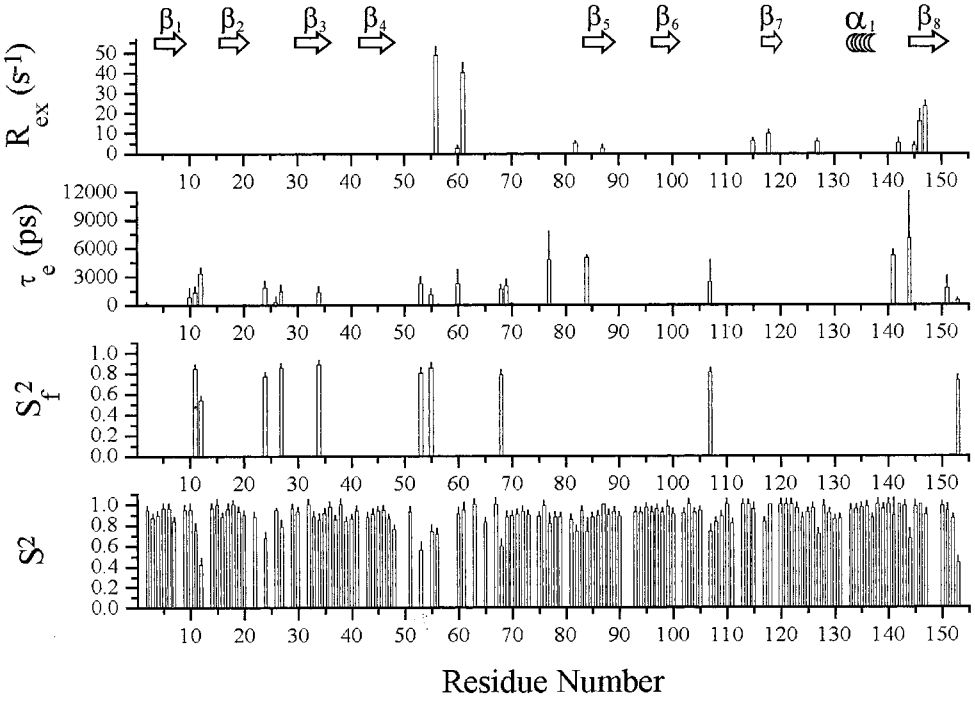

FIGURE 2: Backbone mobility parameters obtained from the model-free analysis for monomeric SOD.

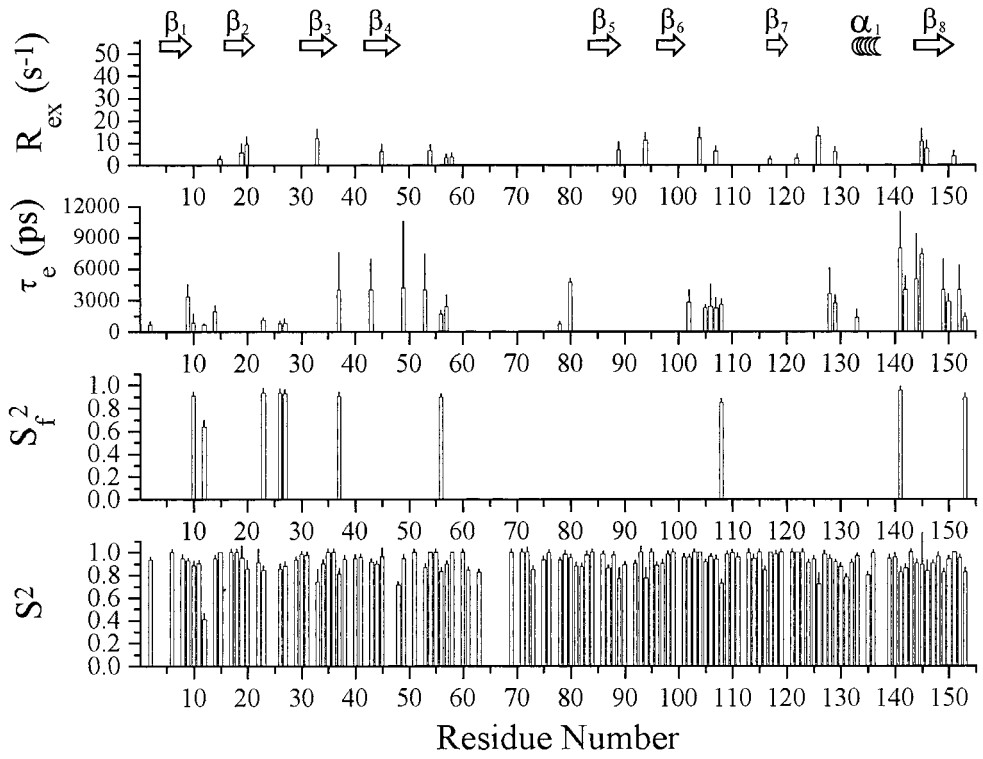

FIGURE 3: Backbone mobility parameters obtained from the model-free analysis for dimeric SOD.

equilibrium. The same behavior is observed for residues 94, 104, 129, 146. Residue 45 shows no dependence of the measured $R_{1\rho}$ rates on the spin-lock power; in this case the R_2 value is close to its average $R_{1\rho}$, and both are significantly larger than the average R_2 for the protein, indicating the presence of conformational exchange occurring on a time scale shorter than 35 μs. The same behavior is observed for residue 89 (which however has R_2 and average $R_{1\rho}$ values much closer than for residue 45 to the average for the rest of protein).

In both analyses the percentage of residues which could not be fitted satisfactorily with Modelfree is about 4-5%, which is in the same range as found for other proteins (*45*).

DISCUSSION

Mobility of the Monomer. For the monomer, the average backbone S^2 value is 0.89 ± 0.11. This indicates that the structure is particularly rigid on the picosecond to nanosecond time scale. This is not unexpected, given the extensive amount of regular β structure constituting the Greek key motif of the protein. Indeed, such a high rigidity of the regions of secondary structure has been reported for other predominantly β-sheet proteins, e.g., fatty acid-binding proteins (*56*, *57*). The last two residues (particularly the C-terminal residue 153) constitute the most flexible region. The most flexible loops are loop I and the first part of loop IV, where point mutations have been introduced. However, within these loops significant differences in the S^2 values of individual residues are observed (see Figure 2). On the other hand, all β strands have similar average S^2 values.

Large (greater than 5 s^{-1}) R_{ex} contributions to the R_2 relaxation rates were individuated from the model-free fittings for residues 56, 61, 115, 118, 127, 146, and 147 (Figure 2). For these residues also the analysis of the ^{15}N $R_{1\rho}$ relaxation rates hinted the presence of conformational exchange processes. SOD contains a disulfide bridge involving cysteines 57 and 146. It is known that conformational exchange processes involving the disulfide bridge may cause the onset of dynamic processes not only for the backbone of the cysteines forming the bridge, but also for neighboring residues (*26*). Indeed, R_{ex} contributions were determined also for residues 60 (ca 3 s^{-1}) and 145 (ca 4 s^{-1}). Residues 57 and 58 were not observed in the spectra of the monomer, as well as the backbone ^{15}N of residue 59 (*42*). The above experimental data suggest that the regions 56−61 and 145−147 undergo conformational exchange processes, possibly linked to isomerization of the disulfide bridge.

Mobility of the Dimer. For the dimer, the average backbone S^2 value is 0.92 ± 0.09, which is essentially the same value as for the monomer. Thus, also in the dimeric form the structure is rigid on the picosecond to nanosecond time scale. The most flexible loop is loop I. However, most of this flexibility is accounted for by residue 12, whose S^2 value is as low as 0.41 (Figure 3). All the β-strands display comparable mobility. Residues having S_f^2 values different from 1.00 are only found in loop regions (loop I, II, III, IV, VI, and VIIb), or at the C-terminus. Also residues for which a τ_e value was determined mainly belong to loops (Figure 3). Overall, from Figure 3 it appears that in dimeric SOD the amplitude of picosecond to nanosecond mobility does not depend strongly on the type of secondary structure. However, motions in the loop regions display longer correlation times than in β strands. Strand β8 is the only significant exception to this general behavior.

More than half of the residues displaying conformational exchange belong to β strands. Indeed, the existence of "breathing" motions in β sheets had been proposed on the basis of ^{15}N relaxation data also for other proteins (*56*, *58*). The analysis of $R_{1\rho}$ data confirms the presence of exchange processes detected by the model-free analysis not only for

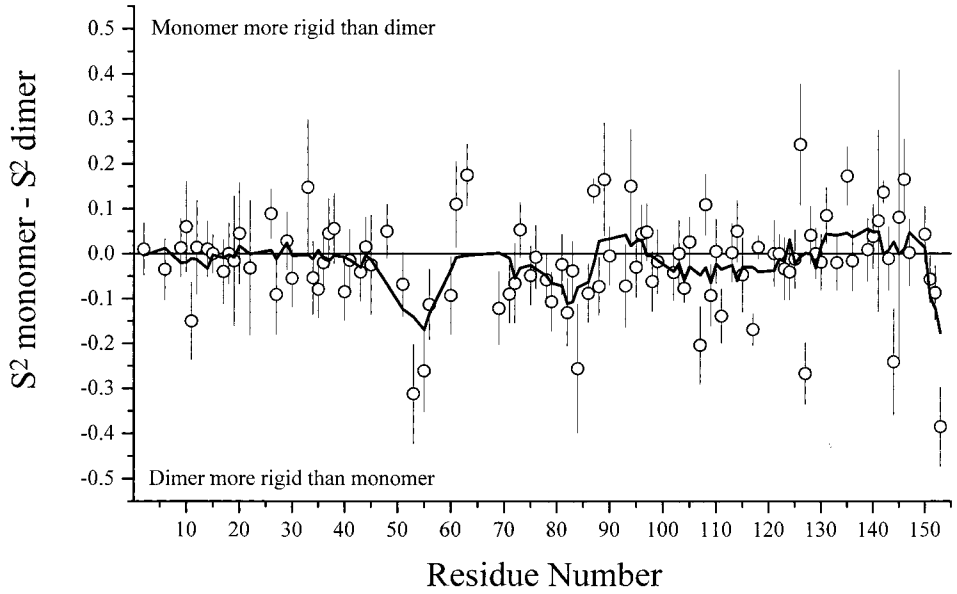

FIGURE 4: Plot of the differences between the S^2 values of monomeric and dimeric SOD. Only residues for which a S^2 value was obtained in both forms are shown (open circles). The thin lines show the uncertainty of each of the differences. The thick line represents a smoothing of the data by averaging over five adjacent points (centered on the point of interest).

the residues with large (greater than 5 s^{-1}) R_{ex} values, but also for many of the residues with R_{ex} values lower than 5 s^{-1}. Among the residues close in sequence to cysteines 57 and 146 (which form a disulfide bridge), R_{ex} values were calculated for residues 54, 57, 58 and 145, 146 (Figure 3). This indicates that some conformational exchange is present in the dimer around the disulfide bridge.

Comparison of the Backbone Dynamics of Monomeric and Dimeric SOD. Figure 4 reports the difference between S^2 values obtained for monomeric and dimeric SOD on a per residue basis. Positive values indicate that the NH vector is more mobile in the dimer, and viceversa for negative values. To highlight regions having different mobility in the picosecond to nanosecond time scale in the two systems, the graph of Figure 4 has been smoothed by averaging over five adjacent points. The regions in the smoothed graph showing the largest decrease in mobility in the dimer with respect to the monomer correspond to residues 47−59, 76−86, 151−153. The regions where instead the monomer is consistently less mobile (although here the differences are smaller in magnitude than in the regions mentioned before) than the dimer are 131−142, and, to a smaller extent, 88−95. The differences in mobility between the two species are also shown graphically in Figure 5.

Regions 47−59 and 151−153 are both at the dimer interface (which encompasses residues 49−54, 113−115 and 148−153). For both regions the monomeric form displays enhanced mobility with respect to the dimer (Figure 5). This can be rationalized by considering that the presence of the second subunit limits the space accessible to the side chains of the residues at the interface, and thus, through the side chains, restricts the mobility of the protein backbone as well. Indeed, the intersubunit interactions of the residues at the interface restrict the number of their energetically accessible conformations (e.g., by contributing a favorable energy to some conformations through hydrophobic interactions with the other subunit, thus increasing the energy gap with other conformations), thereby restricting their mobility. In addition, the increased solvent exposure of the residues at the interface can destabilize hydrophobic amino acids, increasing the energy of their possible conformations and reducing the activation barriers between different conformations. This contribution may be important for the 151−153 region, which comprises mainly hydrophobic amino acids (with the exception of Gln 153). From Figure 4 it can be seen that also the region 102−120 displays, albeit to a minor extent, enhanced mobility in the monomer with respect to the dimer, consistently with the fact that it encompasses the intersubunit contact region 113−115.

The region around 131−142 is more rigid in the monomer than in the dimer (Figures 4 and 5). It lies close to the opening of the active site channel, and encompasses a large part of the so-called electrostatic loop (loop VII). The latter has been shown to play a primary role in guiding the superoxide anion toward the active site (*6*). The 131−142 region is relatively far from the interface, and it seems unlikely that the exposure of the latter can have direct effects on its mobility. The observed change in its mobility may instead be modulated through its interaction with residues 44−48 and 62−63, which are close to the dimer interface. This loop also contains the mutation E133Q in the monomer. However, the S^2 value of residue 133 is the same in the monomer and in the dimer, suggesting that the influence of the mutation of this exposed residue on the mobility of the region is small.

The differences in mobility observed for regions 76−86 and 88−95 are difficult to explain as these regions are far from the dimer interface and not even in close contact with residues close to the interface. Long-range effects are probably responsible for this behavior. However, the currently available data do not allow a satisfactory rationalization of this experimental finding.

As far as conformational exchange is concerned, from the comparison of Figures 2 and 3, it can be seen that in the monomer large R_{ex} values are observed around the regions of the disulfide bridge, while in the dimer the R_{ex} contributions observed for the same residues are sizably smaller, or even absent, with the single exception of residue 145. From

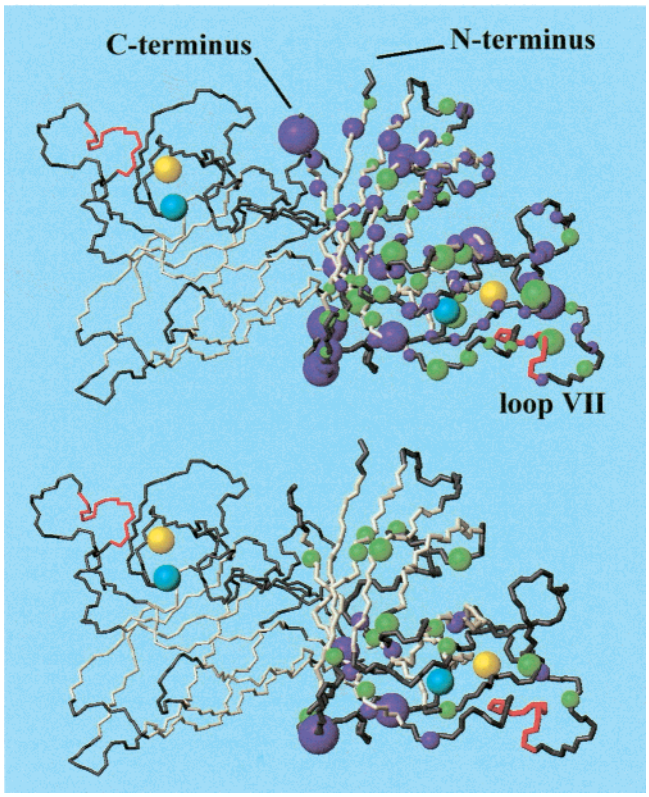

FIGURE 5: Display of the differences in the order parameter (top) and in the R_{ex} (bottom) values between monomeric and dimeric human SOD. Each sphere is centered on the backbone amide nitrogen of the residue considered. Only residues for which relaxation data were available in both forms are displayed. The radius of the sphere is proportional to the value of the difference in S^2 (top) or in R_{ex} (bottom). Residues less mobile (i.e., with larger S^2 or smaller R_{ex}) in the dimer are in purple, whereas residues less mobile in the monomer are in green. The Cu ion is shown in cyan, the Zn ion in yellow. Elements of secondary structure are highlighted (white, β structure; red, α structure). Both subunits are shown, but, for clarity, spheres were only drawn for residues belonging to the first subunit.

the analysis of $R_{1\rho}$ relaxation rates, it appears that for most of the residues in these regions showing conformational exchange, the τ_{ex} of the process is similar in the two systems (in the range of 100−200 μs). It seems reasonable to assume that the differences in ^{15}N chemical shift between the different conformations in equilibrium are similar in the monomer and in the dimer, also based on the fact that the residues in the mentioned regions do not display large changes in chemical shift between the monomer and the dimer. With the above findings and assumptions, from eq 6 it can be deduced that the observed difference in the R_{ex} values reflects a difference in the values of the relative populations of the conformations in equilibrium. In particular, the smaller R_{ex} values observed for the dimer indicate that in this system there is one predominant conformation. Besides the above mentioned residues, in the dimer, at variance with the monomer, there are several other residues having R_{ex} values in the range 5−10 s^{-1}. They are located in strands β2, β3, β4, β5, β7, and β8, and loops IV−VIIa. These data point out to the existence of breathing motions of the SOD β-barrel whose amplitude is somewhat larger in the dimer than in the monomer. Concerted motions of the two subunits may also be involved (*59*, *60*).

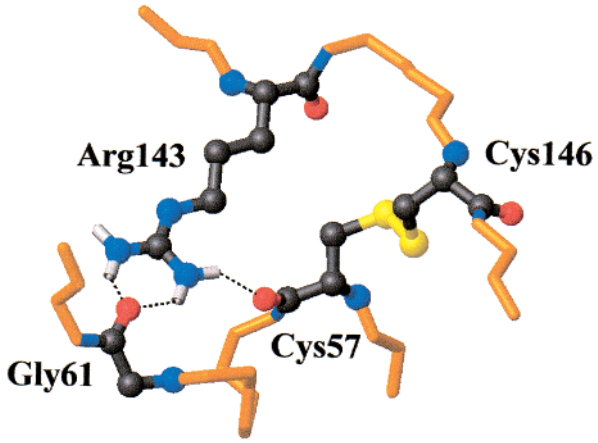

FIGURE 6: Display of the hydrogen bond network responsible for the correct orientation of the side chain of Arg143 in dimeric SOD.

Biological Implications. The enzymatic activity of the monomeric SOD mutant studied here is roughly 20% that of the dimeric enzyme (*13*). The efficiency of SOD depends largely on the electrostatic field of the active site channel, which guides the diffusion of the copper ion toward the copper site [see ref *1* and references therein (*6*, *7*)]. The channel is formed by the electrostatic loop VII, where the charged residues most important for SOD catalysis lie, and loop IV where Cys57 lies (*61*, *62*). In particular, the importance of the correct positioning of the side chain of Arg 143 has been highlighted (*14*, *20*, *63*). This is ensured by the presence of H-bonds between its terminal guanidinic moiety with the backbone oxygen atoms of Cys57 and Gly61 (Figure 6). The results described in the preceding sections provide evidence that in the monomer the region around Cys57 undergoes conformational exchange processes, which instead are less prominent in the dimer. Thus, in the monomer the oxygen atoms of the backbone of residues 57 and 61 sample different orientations in solution. On the contrary, in the dimer a single conformation is prevalent (see preceding section). It is likely that most of the conformers in equilibrium in the monomer (or, possibly, all of them) do not allow Arg143 to assume a functional orientation (either because the hydrogen bond network is broken, or because it is modified in a way such that the side chain of Arg143 is incorrectly positioned), thus reducing the enzymatic activity. The above reasoning is also in agreement with the observed disorder of the side chain of Arg143 in the crystal structure of the present monomeric form (*15*), and with the fact that the resonance of Nϵ atom of Arg143 cannot be observed by NMR, possibly due to exchange broadening (*14*, *42*). On the other hand, the prevalent conformation of the region around residue 57 in the dimer constrains the side chain of Arg143 in the proper, active conformation.

Another contribution to the observed reduced activity of the present monomeric mutant with respect to the dimer may arise from the increased rigidity of the region 131−142. Structural fluctuations in this region may play a role in driving the superoxide anion toward the active site (*23*). It is known that the catalytic process of SOD is limited by the diffusion of superoxide through the active channel. The diffusion coefficient of superoxide is around 100 Å^2 ns^{-1} (*64*). This implies that the superoxide anion can cover a distance of 10 Å (i.e., equal to the depth of the SOD active channel) in a time of the order of nanoseconds. Thus motions

having a correlation time of the order of nanosecond will play a specific role in driving superoxide to the reaction center, faster motions only providing an average effect during the diffusion process. In the dimer, residues 133, 141, and 142 display a τ_e larger than 1 ns, which is in the appropriate range. However, it should be kept in mind that determination of τ_e values may often be unreliable (*44*), and that under conditions (e.g., small percentage of aggregation) where the bias on S^2 values is still acceptable, τ_e values may be sizably overestimated (*31*). It can be thus concluded that, although they do not provide definite evidence, the present data are consistent with a possible role played by fluctuations of the 130−140 region with respect to the enzymatic activity of SOD. This role may be mediated by instantaneous changes of the structure in response to the diffusion of the substrate through the active channel, which facilitate the diffusional process.

The dimeric G37R mutant of SOD is known to be implied in the onset of familial amyotrophic lateral sclerosis (FALS) (*65*). It has been proposed that the role of abnormal SOD in the onset of the disease is related to an enhanced reactivity of the copper site with other substrates besides superoxide in vivo (*66*). Notably, SOD mutants implied in the FALS disease display a superoxide dismutase activity similar to that of the wild-type enzyme (*67*). The G37R mutant has been proposed to have an enhanced mobility of the region 133−144 (*49*), which corresponds to the region displaying enhanced mobility in the dimeric form with respect to the monomeric one. Increased flexibility in the vicinity of the active site channel has been proposed also for other FALS mutants (*68*). It can thus be suggested that the relatively high flexibility of the region 131−142 in FALS SOD mutants may be responsible for the enhanced reactivity of the copper site with respect to other substrates than superoxide (e.g., nitric oxide) by enhancing their diffusion toward the copper ion.

CONCLUSIONS

In this work, the backbone dynamics of a monomeric mutant of human SOD, and of the dimeric enzyme have been characterized and compared. As far as motions in the picosecond to nanosecond time scale are concerned, the regions 47−59, 76−86, and 151−153 were found to be more rigid in the dimer, while the regions 131−142 and, to a smaller extent, 88−95 were found to be more rigid in the monomer. Important conformational exchange processes have been observed in the monomer for regions around cysteines 57 and 146, which form a disulfide bridge. This exchange phenomena are sizably reduced in the dimer. The reduced enzymatic activity of the monomer with respect to the dimer (ca 20%) is postulated to be due mainly to the incorrect positioning of the side chain of Arg143 caused by its non-optimal interaction with residues 57 and 61 in at least some of the conformers involved in the above mentioned exchange equilibrium. The present data are also compatible with a possible influence of the different amplitude of the fluctuations of the electrostatic loop in the two species on the diffusion of the substrate toward the active site and thus on the catalytic rate. This finding may be relevant also for the understanding of the abnormal behavior of SOD FALS mutants in vivo. The influence on the enzymatic activity of the other differences in backbone dynamics observed in this study is unclear, but likely small.

ACKNOWLEDGMENT

We thank Dr. Mario Piccioli for the acquisition and preliminary analysis of the spectra of the monomeric protein.

SUPPORTING INFORMATION AVAILABLE

Backbone ^2H, ^{15}N and ^{13}C resonance assignments for the reduced human SOD at 298 K and pH 5.0; a figure showing relaxation data for typical residues in monomeric and dimeric SOD; two figures showing experimental R_1, R_2 and NOE data for monomeric and dimeric SOD. This material is available free of charge via the Internet at http://pubs.acs.org.

REFERENCES

1. Bertini, I., Mangani, S., and Viezzoli, M. S. (1998) in *Advanced Inorganic Chemistry* (Sykes, A. G., Ed.) pp 127−250, Academic Press, San Diego, CA.
2. McCord, J. M., and Fridovich, I. (1969) *J. Biol. Chem. 244*, 6049−6055.
3. Fee, J. A., and Gaber, B. P. (1972) *J. Biol. Chem. 247*, 60−65.
4. Tainer, J. A., Getzoff, E. D., Richardson, J. S., and Richardson, D. C. (1983) *Nature 306*, 284−287.
5. Banci, L., Bertini, I., Luchinat, C., and Hallewell, R. A. (1988) *J. Am. Chem. Soc. 110*, 3629−3633.
6. Getzoff, E. D., Cabelli, D. E., Fisher, C. L., Parge, H. E., Viezzoli, M. S., Banci, L., and Hallewell, R. A. (1992) *Nature 358*, 347−351.
7. Getzoff, E. D., Tainer, J. A., Weiner, P. K., Kollman, P. A., Richardson, J. S., and Richardson, D. C. (1983) *Nature 306*, 287−290.
8. Klapper, I., Hagstrom, R., Fine, R., Sharp, K., and Honig, B. (1986) *Proteins: Struct., Funct., Genet. 1*, 47−59.
9. Sines, J. J., Allison, S. A., and McCammon, J. A. (1990) *Biochemistry 29*, 9403−9412.
10. Tainer, J. A., Getzoff, E. D., Beem, K. M., Richardson, J. S., and Richardson, D. C. (1982) *J. Mol. Biol. 160*, 181−217.
11. Parge, H. E., Getzoff, E. D., Scandella, C. S., Hallewell, R. A., and Tainer, J. A. (1986) *J. Biol. Chem. 261*, 16215−16218.
12. Bertini, I., Piccioli, M., Viezzoli, M. S., Chiu, C. Y., and Mullenbach, G. T. (1994) *Eur. J. Biophys. 23*, 167−176.
13. Banci, L., Bertini, I., Chiu, C. Y., Mullenbach, G. T., and Viezzoli, M. S. (1995) *Eur. J. Biochem. 234*, 855−860.
14. Banci, L., Benedetto, M., Bertini, I., Del Conte, R., Piccioli, M., and Viezzoli, M. S. (1998) *Biochemistry 37*, 11780−11791.
15. Ferraroni, M., Rypniewski, W., Wilson, K. S., Viezzoli, M. S., Banci, L., Bertini, I., and Mangani, S. (1999) *J. Mol. Biol. 288*, 413−426.
16. Klug, D., Rabani, J., and Fridovich, I. (1972) *J. Biol. Chem. 247*, 4839−4842.
17. Bull, C., and Fee, J. A. (1985) *J. Am. Chem. Soc. 107*, 3295−3304.
18. Bielski, B., and Cabelli, D. (1991) *J. Radiat. Biol. 59*, 291−319.
19. Banci, L., Bertini, I., Luchinat, C., and Viezzoli, M. S. (1993) *Inorg. Chem. 32*, 1403−1406.
20. Fisher, C. L., Cabelli, D. E., Tainer, J. A., Hallewell, R. A., and Getzoff, E. D. (1994) *Proteins: Struct., Funct., Genet. 19*, 24−34.
21. Polticelli, F., Battistoni, A., Bottaro, G., Carri, M. T., O'Neill, P., Desideri, A., and Rotilio, G. (1994) *FEBS Lett. 352*, 76−78.
22. Banci, L., Bertini, I., Viezzoli, M. S., Argese, E., Orsega, E., Choi Ying Chiu, and Mullenbach, G. T. (1997) *J. Biol. Inorg. Chem. 2*, 295−301.
23. Luty, B. A., El Amrani, S., and McCammon, J. A. (1993) *J. Am. Chem. Soc. 115*, 11874−11877.
24. Kay, L. E., Torchia, D. A., and Bax, A. (1989) *Biochemistry 28*, 8972−8979.

25. Clore, G. M., Szabo, A., Bax, A., Kay, L. E., Driscoll, P. C., and Gronenborn, A. M. (1990) *J. Am. Chem. Soc. 112*, 4989−4991.
26. Szyperski, T., Luginbuhl, P., Otting, G., Güntert, P., and Wüthrich, K. (1993) *J. Biomol. NMR 3*, 151−164.
27. Akke, M., and Palmer, A. G., III (1996) *J. Am. Chem. Soc. 118*, 911−912.
28. Lipari, G., and Szabo, A. (1982) *J. Am. Chem. Soc. 104*, 4546−4559.
29. Peng, J. W., and Wagner, G. (1992) *J. Magn. Reson. 98*, 308−332.
30. Woessner, D. E. (1962) *J. Chem. Phys. 3*, 647−652.
31. Schurr, J. M., Babcock, H. P., and Fujimoto, B. S. (1994) *J. Magn. Reson., Ser. B 105*, 211−224.
32. Tjandra, N., Wingfield, P., Stahl, S., and Bax, A. (1996) *J. Biomol. NMR 8*, 273−284.
33. Desvaux, H., Birlirakis, N., Wary, C., and Berthault, P. (1995) *Mol. Phys. 86*, 1059−1073.
34. Grzesiek, S., and Bax, A. (1992) *J. Magn. Reson. 96*, 432−440.
35. Clubb, R. T., Thanabal, V., and Wagner, G. (1992) *J. Magn. Reson. 97*, 213-217.
36. Pervushin, K., Riek, R., Wider, G., and Wüthrich, K. (1997) *Proc. Natl. Acad. Sci. U.S.A. 94*, 12366−12371.
37. Wider, G., Neri, D., Otting, G., and Wüthrich, K. (1989) *J. Magn. Reson. 85*, 426−431.
38. Kay, L. E., Nicholson, L. K., Delaglio, F., Bax, A., and Torchia, D. A. (1992) *J. Magn. Reson. 97*, 359−375.
39. Marion, D., and Wüthrich, K. (1983) *Biochem. Biophys. Res. Commun. 113*, 967−974.
40. Grzesiek, S., and Bax, A. (1993) *J. Am. Chem. Soc. 115*, 12593−12594.
41. Zinn-Justin, S., Berthault, P., Guenneugues, M., and Desvaux, H. (1997) *J. Biomol. NMR 10*, 363−372.
42. Banci, L., Benedetto, M., Bertini, I., Del Conte, R., Piccioli, M., Richert, T., and Viezzoli, M. S. (1997) *Magn. Reson. Chem. 35*, 845−853.
43. Marquardt, D. W. (1963) *J. Soc. Ind. Appl. Math. 11*, 431−441.
44. Palmer, A. G., III, Rance, M., and Wright, P. E. (1991) *J. Am. Chem. Soc. 113*, 4371−4380.
45. Mandel, M. A., Akke, M., and Palmer, A. G., III (1995) *J. Mol. Biol. 246*, 144−163.
46. Lee, L. K., Rance, M., Chazin, W. J., and Palmer, A. G., III (1997) *J. Biomol. NMR 9*, 287−298.
47. Brüschweiler, R., Liao, X., and Wright, P. E. (1995) *Science 268*, 886−889.
48. Tjandra, N., Feller, S. E., Pastor, R. W., and Bax, A. (1995) *J. Am. Chem. Soc. 117*, 12562−12566.
49. Hart, P. J., Liu, H., Pellegrini, M., Nersissian, A. M., Gralla, E. B., Valentine, J. S., and Eisenberg, D. (1998) *Protein Sci. 7*, 545−555.
50. Deng, H.-X., Hentati, A., Tainer, J. A., Lqbal, Z., Cyabyab, A., Hang, W.-Y., Getzoff, E. D., Hu, P., Herzfeldt, B., Roos, R. P., Warner, C., Deng, G., Soriano, E., Smyth, C., Parge, H. E., Ahmed, A., Roses, A. D., Hallewell, R. A., Pericak-Vance, M. A., and Siddique, T. (1993) *Science 261*, 1047−1051.
51. Halle, B., and Wennerström, H. (1981) *J. Phys. Chem. 75*, 1928−1943.
52. Barbato, G., Ikura, M., Kay, L. E., Pastor, R. W., and Bax, A. (1992) *Biochemistry 31*, 5269−5278.
53. Davis, D. G., Perlman, M. E., and London, R. E. (1994) *J. Magn. Reson., Ser. B 104*, 266−275.
54. Copié, V., Tomita, Y., Akiyama, S. K., Aota, S., Yamada, K. M., Venable, R. M., Pastor, R. W., Krueger, S., and Torchia, D. A. (1998) *J. Mol. Biol. 277*, 663−682.
55. James, T. L., Matson, G. B., Kuntz, I. D., and Fisher, R. W. (1977) *J. Magn. Reson. 28*, 417−426.
56. Cheng, J. W., Lepre, C. A., Chambers, S. P., Fulghum, J. R., Thomson, J. A., and Moore, J. M. (1993) *Biochemistry 32*, 9000−9010.
57. Hodsdon, M. E., and Cistola, D. P. (1997) *Biochemistry 36*, 2278−2290.
58. Redfield, C., Boyd, J., Smith, L. J., Smith, R., and Dobson, C. M. (1992) *Biochemistry 31*, 10431−10437.
59. Falconi, M., Gallimbeni, R., and Paci, E. (1996) *J. Comput. Aided Mol. Des. 10*, 490−498.
60. Chillemi, G., Falconi, M., Amadei, A., Zimatore, G., Desideri, A., and Di Nola, A. (1997) *Biophys. J. 73*, 1007−1018.
61. Getzoff, E. D., Tainer, J. A., Stempien, M. M., Bell, G. I., and Hallewell, R. A. (1989) *Proteins: Struct., Funct., Genet. 5*, 322−336.
62. Parge, H. E., Hallewell, R. A., and Tainer, J. (1992) *Proc. Natl. Acad. Sci. U.S.A. 89*, 6109−6114.
63. Banci, L., Bertini, I., Del Conte, R., Mangani, S., and Viezzoli, M. S. (1999) *J. Biol. Inorg. Chem. 4*, 795−803.
64. Sharp, K., Fine, R., and Honig, B. (1987) *Science 236*, 1460−1463.
65. Wong, P. C., Pardo, C. A., Borchelt, D. R., Lee, M. K., Copeland, N. G., Jenkins, N. A., Sisodia, S. S., Cleveland, D. W., and Price, D. L. (1995) *Neuron 14*, 1105−1116.
66. Smith, C. D., Carson, M., van der Woerd, M., Chen, J., Ischiropoulos, H., and Beckman, J. S. (1992) *Arch. Biochem. Biophys. 299*, 350−355.
67. Borchelt, D. R., Lee, M. K., Slunt, H. S., Guarnieri, M., Xu, Z. S., Wong, P. C., Brown, R. H., Price, D. L., Sisodia, S. S., and Cleveland, D. W. (1994) *Proc. Natl. Acad. Sci. U.S.A. 91*, 8292−8296.
68. Goto, J. J., Zhu, H., Sanchez, R. J., Gralla, E. B., and Valentine, J. S. (2000) *J. Biol. Chem. 14*, 1007−1014

BI000067Z